Small-angle scattering of microparacrystal-bundles in cold-drawn and annealed isotactic polypropylene

A. Ferrero and E. Ferracini
Consiglio Nazionale delle Ricerche, Via Selmi 2, 40126 Bologna, Italy

and R. Hosemann
Gruppe Parakristallforschung, c/o BAM, Unter den Eichen 44-66, 1000 Berlin 45, West Germany
(Received 15 February 1984; revised 17 May 1984)

Sheets of isotactic polypropylene (PP) (thickness 1 mm) were heated above the melting point to about 175°C and quenched in ice water. After this procedure the sheets were cold-drawn at 21°C up to a stretching ratio of 9 and then annealed at 155°C for 24 h in a vacuum with fixed ends. The 50 Å equatorial reflections disappear during annealing, the long period increases from 100 to 255 Å and the lengths of the microparacrystals (mPC's) in the fibre direction increase from 40 to 135 Å. The paracrystalline distortions of the macrolattice decrease drastically during annealing and, consequently, the sizes of the clusters or aggregations of the microparacrystals (lamellae bundles) increase to $3.5 \times 5 \times 5 = \sim 87$ mPC's. A new method of analysing the small-angle scattering is introduced which includes convolution with the shape factor of the bundles by means of measuring the lateral integral widths of the reflection tails. This method leads directly to approximated values of all essential parameters. Final fitting of the experimental curves is carried out by adapting these parameters definitely. As a result of the high resolution of the small-angle camera it is the first time that the tail of zero reflections could be measured. The meridional reflection has an exceptionally small value of $g_{33} = 0.09$. As the microparacrystals are strongly shifted against each other in the fibre direction ($g_{r3} = 0.14$), one has to conclude that they are not aggregated smectic-like as in lamellae bundles, but nematic-like as in fibrous materials. This may be understood by taking into consideration that the annealing process occurred with fixed ends.

(Keywords: aggregation; macroparacrystals; amorphous phase density; microparacrystals (mPC's); polypropylene (PP); shape factor; zero reflection)

INTRODUCTION

The two-dimensional small-angle diffraction analysis of well oriented fibrous structures of polymers leads to novel structure parameters not accessible in unoriented samples. The first attempt was made by a one-dimensional analysis of the meridional reflection of linear polyethylene with help of the theory of paracrystals[1]. The diffraction of microparacrystals (mPC's) which build up a three-dimensional lattice in a fibrous arrangement, could be calculated by means of zero-order Bessel functions[2]. A two-dimensional SAXS pattern was first analysed from isotactic polybutene stretched from the melt[3], using an approximation along the meridian and orthogonal to it along the meridional reflection. A similar analysis, but along the equator and parallel to the meridian, of monoclinic isotactic polypropylene was published in 1976[4]. Hot-stretched polyethylene has been analysed in the same way with computer calculated best fits[5], showing that the general model of paracrystalline lamellae of J. J. Hermans[6], which avoids overlapping of lamellae, gives approximately the same results as for the paracrystalline model[7]. Further information can be obtained with help of a small-angle camera for absolute intensity measurements[8].

In the following sections the above mentioned isotactic polypropylene is described after additional annealing for 24 h with fixed ends in temperature range III where a melting of the lateral grain boundaries of the microparacrystals takes place[9]. The 50 Å equatorial reflections disappear. Novel equations are shown which facilitate analysis by introducing the shape factor of the aggregations (bundles) of microparacrystals and the integral widths of the K_k discs of the paracrystalline lattice factor.

EXPERIMENTAL

Samples

Sheets of isotactic PP (1 mm thick) were heated at about 175°C, above its melting point, and quenched in a dry ice–acetone mixture. The samples were cold-drawn at 21°C up to a stretching ratio of 9 and annealed for 24 h in vacuum at 155°C with fixed ends to avoid shrinkage which is followed by partial disorientation of the relative fibre patterns. The annealing temperature (155°C) is very near to the melting point of the unannealed samples (158°C) measured by a microcalorimeter.

SAXS camera

SAXS measurements were made using a high resolution camera with pinhole collimation with a resolution power

0032-3861/84/121747-08$03.00

of 1230 Å on the beam stop edge and a resolution of 4550 Å relatively to the half-width of the primary beam ($b=2.2\times10^{-4}$ Å^{-1}). Deconvolution with the primary beam was not necessary since its width was 5 times or more smaller than the width of the reflection. The sample-recording plane distance was 39.9 cm. PP samples annealed at a temperature near the melting point show, in comparison with unannealed samples[4], equal SAXS diagrams both when the X-rays are perpendicular or parallel to the sheets. Here the analysis of the superstructure of stretched and annealed PP is performed taking into account the three-dimensional structure of the paracrystalline lattice factor $Z(h)$ in the small-angle scattering domain and the size of the bundles. Ni filtered CuKα radiation from rotating anode Rigaku Generator was employed.

Owing to the high resolution of the SAXS camera, the influence of the white radiation scattered at very low angles was remarkable, and consequently a correction was performed in the fibre direction of the SAXS spectra using the scattering of paraffin $C_{24}H_{50}$ recorded under the same conditions as for the PP samples. Paraffin was highly oriented after annealing at 49°C for 47 h between two glass plates. The broken line in *Figure 3* denotes the contribution of the white radiation.

Other measurements

The crystalline density ρ_c was calculated from the lattice cell dimensions measured by wide-angle X-ray diffraction using an AEG Guinier-Jagodzinski camera with a focussing monochromator which completely eliminates the CuKα_2 radiation.

The crystallinity of the samples was determined both from SAXS data and from broad-line nuclear magnetic resonance (n.m.r.), Using a Varian V-4200 B spectrometer with a WL 112 console.*

Macroscopic density measurements were carried out using the combined floatation and pycnometer method.

N.m.r. data. The mass crystallinity (rigid chain segments) is

$$\alpha=59.5\pm0.6\%$$

and the amorphous parts (mobile segments) are

$$\beta_1=37.4\pm0.5\%$$
$$\beta_2=3.0\pm0.1\%$$

From WAXS the crystalline density is $\rho_c=0.9406$ g cm^{-3}. The measured *macroscopic density* is $\rho=0.9135$ g cm^{-3}, from which the *volume crystallinity* and the density of the 'amorphous phase' can be calculated as $\alpha_v=\rho/\rho_c=57.7\%$

$$\rho_a=0.877\text{ g cm}^{-3}$$

which is almost the same as for atactic PP (0.85 g).

THE GENERALIZED INTENSITY FUNCTION

The intensity function of crystals is, according to M. V. Laue and P. P. Ewald, defined by

$$I(\underline{b})=N(\bar{f}^2-\bar{f}^2)+\frac{1}{v_r}\bar{f}^2\widehat{ZS}^2;\quad \underline{b}=\frac{\underline{s}-\underline{s}_0}{\lambda} \tag{1}$$

where $\underline{s}$ and $\underline{s}_0$ are unit vectors in the direction of the scattered resp. primary beam, λ the wavelength and v_r the volume of a lattice cell. f^2 is the structure factor, S^2 the shape factor of a crystal and Z the lattice peak function. If $\underline{a}_k$ ($k=1,2,3$) are the edges of a lattice cell, then according to the Laue conditions

$$\underline{a}_k\underline{b}=h_k^\circ;\qquad h_k^\circ \text{ integers, } k=1,2,3 \tag{2}$$

are the lattice points of the reciprocal lattice cells and

$$Z(\underline{h})=\sum_{pqr}P(\underline{h}-ph_1^\circ-qh_2^\circ-rh_3^\circ) \tag{3}$$

is the peak function according to P. P. Ewald with

$$\int P(\underline{h})\,\mathrm{d}h^3=1;\qquad P(\underline{h})=0 \text{ if } h>\varepsilon \tag{4}$$

ε is infinitesimally small and $\widehat{ZS}^2=\int Z(\underline{c})S^2(\underline{b}-\underline{c})\mathrm{d}c^3$. Non-crystalline material consists, in all cases investigated until now, of microparacrystals (mPC's). $\underline{a}_k$ fluctuates statistically with an '*a priori* statistic' ($H_k(\underline{x})$ with reference to the ideas from P. Debye.

$$\int H_k(\underline{x})\mathrm{d}x^3=1;\qquad \int\underline{x}H_k(x)\mathrm{d}x^3=\bar{a}_k$$
$$\Delta^2a_{ki}=\frac{1}{\bar{a}_i^2}\int H_k(\underline{x})(\underline{x}-\underline{a}_k,\underline{a}_i)^2\mathrm{d}x^3 \tag{5}$$

The variance relative to $\bar{a}_i$ is given by

$$g_{ki}=\frac{1}{\bar{a}_i}\Delta a_{ki} \tag{6}$$

The lattice peak function is given by

$$Z=Z_1Z_2Z_3;\qquad Z_k=\frac{1-G_k^2}{(1-G_k)^2+4G_k\sin^2\pi h_k} \tag{7}$$

where

$$G_k=|F_k| \text{ and } F_k(\underline{b})=\mathcal{F}H_k(x)\sim G_ke^{-2\pi i\underline{b}\bar{a}_k}$$
$$G_k\sim\exp\left(-2\pi^2\sum g_{ki}^2h_i^2\right) \tag{8}$$

We will describe in future all functions and relations in the dimensionless $\underline{h}$-space by replacing the components b_k by

$$h_k=a_kb_k \tag{9}$$

The three terms $Z_k(\underline{h})$ are three-dimensional functions of the $\underline{h}$-space and represent discs which at $\underline{h}=h_k^\circ$ have maximum values

$$Z_k(h_k^\circ)=\sim\frac{1+G_k}{1-G_k} \tag{10}$$

and minimum values at $h_k=h_k^\circ+1/2$

$$Z_k(h_k^\circ+1/2)\sim\frac{1-G_k}{1+G_k} \tag{11}$$

* We are indebted to Dr J. Loboda-Čačković for carrying out these measurements.

The function

$$U_k(\underline{h}) = \frac{1 - G_k(\underline{h})}{1 + G_k(\underline{h})} \tag{12}$$

is the diffuse background of $Z_k(\underline{h})$ and well defined in the $\underline{h}$-space. The integral value of the disc Z_k at $h_k = h_k^\circ$ is given by

$$\int_{h_k^\circ - 1/2}^{h_k^\circ + 1/2} Z_k(h_k)\mathrm{d}h_k = 1 \tag{13}$$

We will now separate Z_k into the background component U_k and the part of the disc R_k which stands above U_k

$$Z_k = U_k + R_k \tag{14}$$

From equations (10) and (11) one obtains the maximum value $R_k(h_k^\circ)$ of $R_k(h_k)$ which is the difference between the values from equations (10) and (11)

$$R_k(h_k^\circ) = \frac{4G_k}{1 - G_k^2} \tag{15}$$

The integral value of $R_k(\underline{h})$ is given by

$$\int_{h_k^\circ - 1/2}^{h_k^\circ + 1/2} R_k(h_k)\,\mathrm{d}h_k = \frac{2G_k}{1 + G_k} \tag{16}$$

This value divided through equation (15) defines the integral width δ_k of R_k

$$\delta_k = 1/2(1 - G_k) \sim \pi^2 \sum_i g_{ki}^2 h_i^{\circ 2} \tag{17}$$

Now we have to convolute with S^2. For convenience we replace $S^2(h)$ in equation (1) with the product of the terms $S_k(h_k)$ which depend solely on h_k and obtain for its integral width β_k

$$S^2 = S_1^2 S_2^2 S_3^2;\ S_k^2(0) = N_k^2;\ \int S_k \mathrm{d}h_k = N_k, \text{ hence } \delta_k = \frac{1}{N_k} \tag{18}$$

The discs $R_k(h_k)$ in microparacrystals have Cauchy-like shapes. The integral width δ_k of the folding product S_k^2 with $R_k(h_k)$ is then given to a good approximation by the sum of both integral widths, hence

$$\delta_k = \frac{1}{N_k} + \pi^2 \sum_i g_{ki}^2 h_i^{02} \tag{19}$$

All these relations are well established by studies of wide-angle scattering of non-crystalline samples such as solid catalysts, synthetic polymers or melts. We would now like to apply them to the small-angle scattering (SMAS) of high polymers with fibrous textures.

SMAS THEORY OF ORIENTED POLYMERS

The intensity function $I(\underline{b})$ of equation (1) can also be applied to the SMAS of colloidal systems. If all domains of the sample are parallelized with its h_3-axis, but statistically twisted around it, then within a plane $h_3 = \text{constant}$, the family of discs Z_1 and Z_2 can be observed which are drawn orthogonally to each other in *Figure 1*. The axes $\underline{a}_k$ of equation (2) are now expanded between the centres of single microparacrystals (mPC's) with lengths of 50 Å or more. The standard deviations g_{12}, g_{11}, g_{21} and g_{22} in most polymers are so large that only the discs $Z_1(h_1^\circ = 0$ and $Z_2(h_2^2 = 0)$ contribute to the SMAS. This means that solely meridional reflections (O,O,h_3) are observable (*Figure 2*). In most cases $G_1 \sim G_2$ and one therefore obtains

$$G_r(\underline{h}) = G_1(\underline{h}) = G_2(\underline{h}) = \exp[-2\pi^2(g_{rr}^2 h_r^2 + g_{r3}^2 h_3^2)] = G_r(h_r, h_3);\ h_r = \sqrt{h_1^2 + h_2^2} \tag{20}$$

Averaging over a circle with the radius h_r (*Figure 1*) one has to differentiate three components of the averaged function

$$\overline{Z_1 Z_2} = \overline{(U_1 + R_1)(U_2 + R_2)} \tag{21}$$

(a) $\overline{U_1 U_2}$ is, according to equations (9) and (12) given by

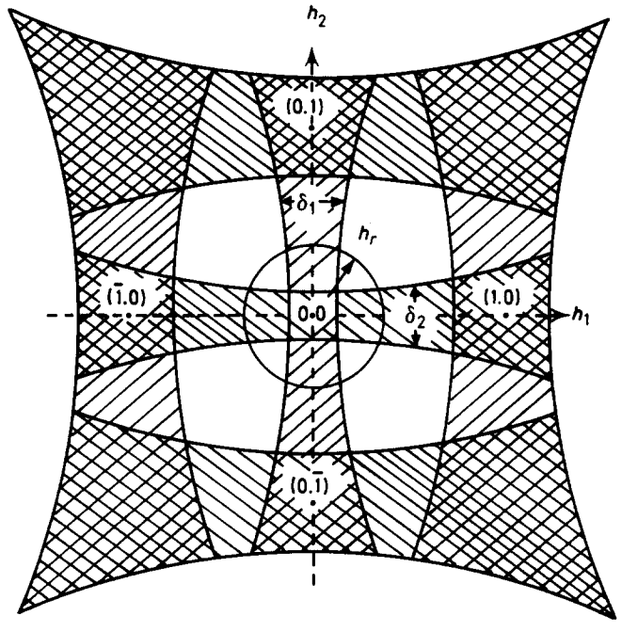

Figure 1 Lattice function $Z_1 Z_2$ of a paracrystalline macrolattice of microparacrystals parallel to the equator at $h_3 = \text{const}$. The peak (0,0, ±1), called the 'long period', is observable as a single peak due to the smoothness of all other peaks

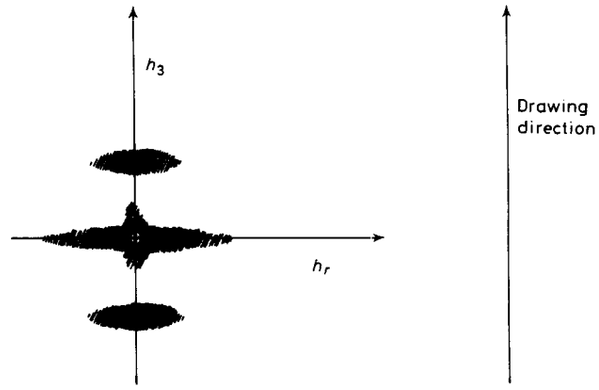

Figure 2 Schematic drawing of the SAXS pattern of 9-fold stretched and then annealed isotactic polypropylene

(b) $$\overline{U_1U_2}=\left(\frac{1-G_r}{1+G_r}\right)^2 \quad (22)$$

$\overline{R_1R_2}$ has according to *Figure 1* and equation (12) values different from zero only for

$$h_r \lesssim \delta_r = \pi^2 g_{r3}^2 h_3^2 + \frac{1}{N_r} \text{ since } h_r^\circ = 0 \quad (23)$$

Its maximum value at $h_r=0$ is given by the square of equation (15). Introducing equation (17) here, one obtains an equation which is important in subsequent calculations

$$\overline{R_1R_2}(0,h_3)=\left(\frac{2G_1}{1+G_1}\cdot\frac{1}{\delta_1}\right)\left(\frac{2G_2}{1+G_2}\cdot\frac{1}{\delta_2}\right)(0,h_3) \quad (24)$$

and

$$\overline{(Z_1Z_2)}(\widehat{S_1^2S_2^2})=\widehat{Z_rS_r^2}=A_r^2=\left[\frac{N_r}{1+G_r}(2G_r/\delta_r+1-G_r)\right]^2 \quad (25)$$

(c) $\overline{(U_1R_1+U_2R_2)}$ has a maximum value

$$\frac{4G_2\delta_r}{(1+G_r)^2}\left(\frac{1}{\delta_1}+\frac{1}{\delta_2}\right) \text{ if } h_r \leqq \delta_r \quad (26)$$

For larger h_r-values one obtains

$$\frac{16G_r\delta_r}{(1+G_r)^2}\cdot\frac{\delta_r}{\pi h_r} \text{ if } \pi h_r > \delta_r \quad (27)$$

because along the h_r-circle one has to integrate through either of the discs twice and obtain four times the value $2U(1-U)/(1+U)$ as the product of equations (12) and (16). This result has to be multiplied by the integral width δ_r of one disc divided through the periphery $2\pi h_r$ of the circle. From equations (1), (8) and (24) we derive

$$I=N(\overline{f^2}-\bar{f}^2)+\bar{f}^2\widehat{(\overline{Z_1Z_1})}(S_2^1S_2^2)Z_3S_3 \quad (28)$$

where f^2 is the scattering function of a microparacrystal. If we approximate f^2 for convenience by cubes with edge lengths D_k, then

$$f^2(\underline{h}) \sim \exp\left(-\frac{\pi^2}{3}\sum_i D_i^2h_i^2\right) \quad (29)$$

In the particular case of an existing isotropy in the lateral direction one obtains

$$I(0,h_3) \cong \exp-\frac{\pi^2}{3}(D_3^2h_3^3+D_r^2h_r^2)\cdot A_r^2\cdot\widehat{Z_3S_3^2} \quad (30)$$

Besides this function we will discuss in the following, details of δ_k-values and Gaussian approximations of other patterns parallel either to the meridian (h_r=constant) or to the equator (h_3=constant).

RESULTS

In previous investigations[3-5] the analysis was performed by introducing, in some cases, a bimodal distance statistic $H(x)$ related to the statistical interruption of the macrolattice. This fact can be interpreted by the empirical parameter α*[11] which relates to the mean size of the microparacrystal bundles and the corresponding paracrystalline fluctuation g_{ik}.

In the present work the SAXs analysis is performed by introducing the shape factor of the above mentioned microparacrystal bundles.

Analysis in meridional direction: the widths $\delta_3(0,1)$ and $\delta_3(h_r,0)$

In *Figure 3* the observed SAXS intensity is drawn along the meridian $(0,h_3)$. The long period reflection at $h_3=1$ is extremely sharp and corresponds to a macrolattice axis of

$$\underline{a}_3 = 260 \text{ Å} \quad (31)$$

The integral width has a value $\delta b_3 \sim 1.3\times10^{-3}$ Å^{-1}. The mean size B_3 of the microparacrystal bundles is therefore given by

$$B_3=\frac{1}{\delta b_3}\cong 775 \text{ Å} \quad (32)$$

After introducing dimensionless coordinates we obtain for the number of microparacrystals in the fibre direction

$$M_3 = 775/260 = 3 \quad (33)$$

We propose that this cannot be the correct number of microparacrystals in the fibre direction because the integral width of the reflection is given by

$$\delta h_3(0,h_3)=\frac{1}{M_3}=\frac{1}{N_3}+\pi^2g_{33}^2h_3^2 \text{ (along the meridian)} \quad (34)$$

The correct number, N_3, of microparacrystals within a bundle or macroparacrystals can be easily determined by analysing the line width δh_3 of the equatorial scattering in the fibre direction. The formula holds:

$$\frac{1}{M_3}=\delta h_3(h_r,0)=\frac{1}{N_3}+\pi^2g_{r3}^2h_3^2 \text{ (along the equator)} \quad (35)$$

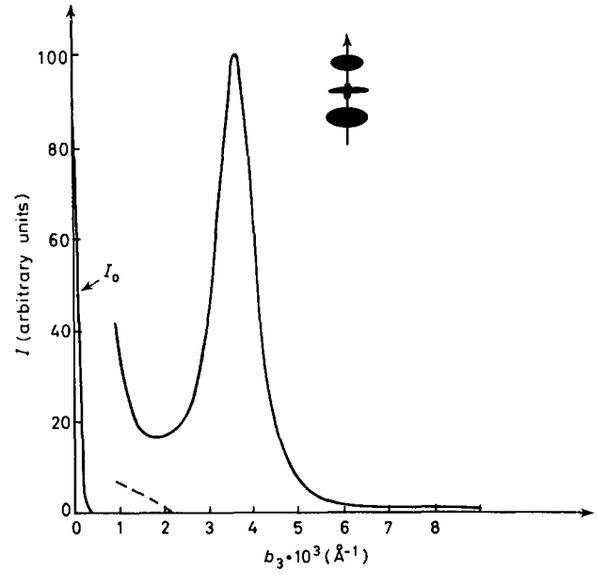

Figure 3 Observed SAXS intensity along the meridian $I(0,h_3)$. I_o is the primary beam profile

Figure 4 shows at $h_r = 8.5 \times 10^{-3}$ a Guinier plot which is very close to the primary beam. There exist two terms: The outer slope leads to $M'_3 = 4$ and the inner tail to $M''_3 = 11$. Taking into account the maxima of the two components, one obtains $M_3 = 5.6$ (see Appendix).

Here the value $(\pi g_{r3} h_3)^2$ in every case is small compared with $1/N_3$ because we discuss the intensity $h_3 = 0$ near the equator. Thus we get

$$N_3 = 5.6 \tag{36}$$

Now we can introduce the value of N_3 to equation (34) and consequently determine the contribution of g_{33} to the integral width $\delta h_3 = 1/M_3$. From equation (34) we obtain, for $h_3 = 1$,

$$\pi^2 g_{33}^2 = \frac{1}{3} - \frac{1}{5.6} = 0.155$$

hence

$$g_{33} = 12.5\% \tag{37}$$

There exists a fundamental equation for microparacrystals which can be applied to macroparacrystals also. It defines the number N of netplanes within a paracrystalline lattice or superlattice as a function of g. For lattice constants smaller than 5 Å this α^*-law is defined by[11]

$$\sqrt{N} g \sim \alpha^*; \qquad \alpha^* = 0.15 \pm 0.05$$

In our case we obtained an extremely high value $\alpha^* = 0.29$ as a consequence of the large lattice constant $a_3 = 260$ Å. In the case of 70S ribosomes with macrolattice cells of $(400 \times 550 \times 420)$ Å^3, however, we found an extremely small value $\alpha^* = 0.07$[13]. Nevertheless, it is interesting to note that for microlattices the deviation of the α^*-value is not as high as it is for macroparacrystals[13].

Analysis in equatorial direction: the widths $\delta_r(0.1/3)$ and $\delta_r(0.1)$

A similar procedure has been performed with SAXS traces parallel to the equator at $h_3 = 1/3$ and $h_3 = 1$. In *Figures 5* and *6* the Guinier plots of the observed intensity functions $I(h_r, 1/3)$ and $I(h_r, 1)$ are drawn. From the outer tails in *Figures 5* and *6* one gets for the diameter (or lateral extension) D_r of the microparacrystals the values $D'_r = 90$ Å and $D''_r = 80$ Å respectively, hence

$$D_r \cong 85 \text{ Å}$$

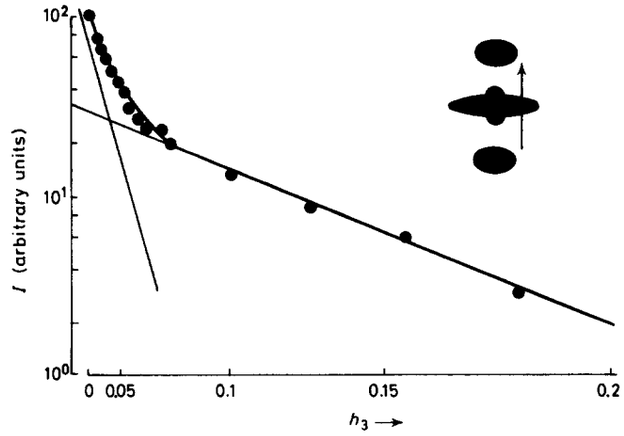

Figure 4 Guinier plot of $I(h_r, h_3)$ with $h_r = 8.5 \times 10^{-3}$ A^{-1} parallel to the meridian

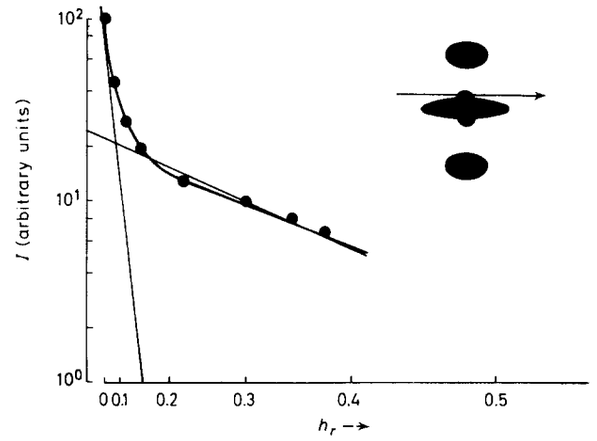

Figure 5 Guinier plot of $I(h_r, 1/3)$

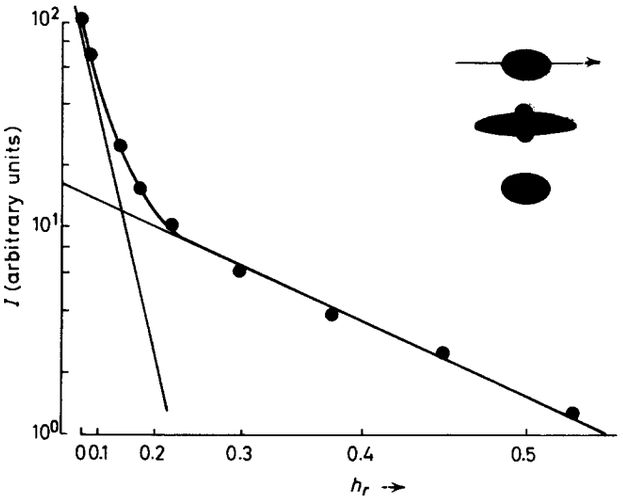

Figure 6 Guinier plot of $I(h_r, 1)$

Assuming that the micropraracrystals are densily packed in the lateral direction we achieve for the lateral cell edges of the macrolattice

$$\underline{a}_r = 85 \cdot 1/2 \cdot \sqrt{3} = 75 \text{ Å}$$

Now we introduce again the dimensionless quantity $h_r = a_r b_r$ for the lateral dimensions of the structure. The inner Gaussian terms of *Figures 5* and *6* make evident the lateral mean size of the microparacrystal bundles, in other words, their dependence on the lateral size of the macroparacrystals. According to equation (35) the relation

$$\delta h_r = \frac{1}{M_r} = \frac{1}{N_r} + \pi^2 g_{r3}^2 h_3^2 \tag{38}$$

holds and leads to

$$M_r(0 \cdot 1/3) = 6.3; \qquad M_r(0.1) = 3.5$$

Substituting $h_3 = 1/3$ and $h_3 = 1$ into equation (38) we obtain as the difference between these two equations

$$\frac{1}{3.5} - \frac{1}{6.3} = (\pi g_{r3})^2 (1 - 1/9), \text{ hence } (\pi g_{r3})^2 = 0.147 \tag{39}$$

$$g_{r3} = 12\%, \qquad N_r = 7, \qquad \alpha^* = \sqrt{N_r} g_{r3} = 0.31$$

It is remarkable that again α^* has the same large value as calculated above for $\sqrt{N_3}g_{33}$.

Direct calculation of $Z_3S_3^2$

As a first step we have evaluated the parameters N_r, N_3, g_{r3} and g_{33} directly from the integral widths of the SAXS patterns. The values obtained from direct calculation are reported in *Table 1*.

It is now possible to perform direct calculation of $\widehat{Z_3S_3^2}$. From a comparison of the calculated and observed $\widehat{Z_3S_3^2}$ values we obtain both a confirmation and a refinement of the values of parameters derived directly from the experimental data. First of all we calculate the term A_r^2 (see equation (25)):

$$A_r^2 = \widehat{Z_rS_r^2} = \left[\frac{N_r}{1+G_r}(2G_r/\delta_r + 1 - G_r)\right]^2 \qquad (40)$$

The outer tail ($h_3 \gg 1$) of *Figure 3* depends practically only on f^2 and we obtain from *Figure 7* (see equation (29)):

$$f^2 = \exp - 1/3(\pi D_3 h_3)^2; \qquad D_3 = 135 \pm 15 \text{ Å} \qquad (41)$$

Following equations (1) and (28), and neglecting as a first approximation the first term of equation (28), the quotient

$$I_{obs}(0,h_3)/(A_r\bar{f})^2 = \widehat{Z_3S_3^2}_{obs} \qquad (42)$$

is calculated.

In *Figure 8* the $\widehat{Z_3S_3^2}_{obs}$ obtained in this way is plotted (broken line), in addition to the observed $I(0,h_3)$ (continuous heavy line) and $\widehat{Z_rS_r^2}x\bar{f}^2$ (–·–·–). The maximum is shifted towards the higher h_3-values and this leads to the exact value of the superlattice parameter a_3:

$$a_3 = 255 \text{ Å} \qquad (43)$$

If we introduce the values a_3, g_{33} and N_3 from equations (36), (37) and (43) we are able to calculate $Z_3S_3^2$ with help of equations (7), (8) and (29). After this procedure all three parameters a_3, g_{33} and N_3 can be varied in order to find the best adapted parameters. The best fit is reported in *Figure 9* (open circles) in comparison with the observed $Z_3S_3^2$ (continuous line) (see *Figure 8*). The calculations, also including the refinement both of A_r^2 and $\widehat{Z_3S_3^2}$ were performed using a computer program. In this final step the term $N(\overline{f^2} - \bar{f}^2)$ from equation (28) has been taken into account. The final macrolattice parameters, relative to the best fit, are reported in *Table 2* in comparison with the corresponding parameters of the unannealed PP[4].

Table 1 Macrolattice parameters as directly derived from experimental SAXS patterns

B_3	775 Å
D_3	128 Å
D_r	85 Å
a_3	260 Å
$\overline{a_r}$	75 Å
$\overline{g_{33}}$	12.5%
g_{r3}	12 %
N_3	5.6
N_r	7

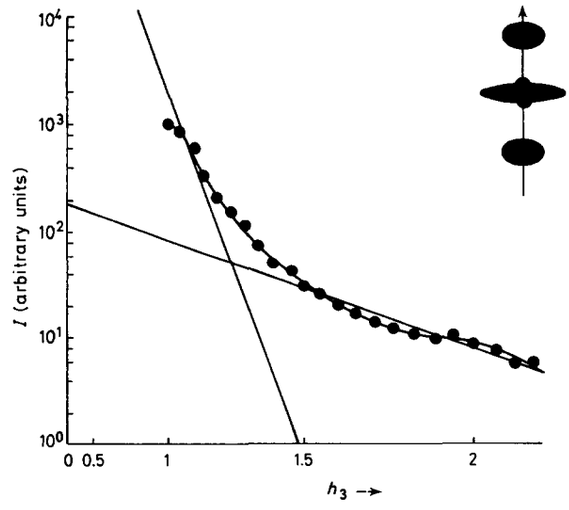

Figure 7 Guinier plot of $I(0,h_3)$. $h_3 \geqslant 1$

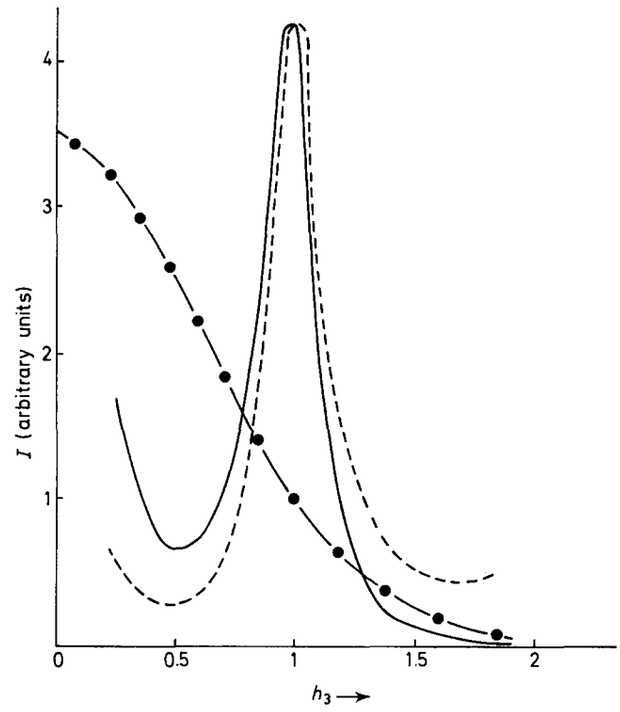

Figure 8 Macrolattice functions along the meridian; SAXS observed intensity $I(0, h_3)$; (———) and calculated $\widehat{Z_3S_3^2}$ (———) and $\widehat{f^2Z_rS_r^2}$ (–·–·–)

DISCUSSION

Table 2 shows the parameters of the monoclinic macrolattice of cold-drawn sheets of isotactic PP[4] and those after annealing at 155°C for 24 h in a vacuum with fixed ends. The final results were obtained using the total intensity formula (equation (28)), starting at the values given in *Table 1* and fitting the whole curve by adapting these values. In this way an exact measurement of the polydispersity g_H of the microparacrystal length (D_3) is possible:

$$g_D = (\overline{D^2}/\bar{D}^2 - 1)^{1/2}; \qquad g_D = 19\% \qquad (44)$$

From *Table 2* it can be recognized that the 'long period' a_3 and the length D_3 of the microparacrystals in the fibre

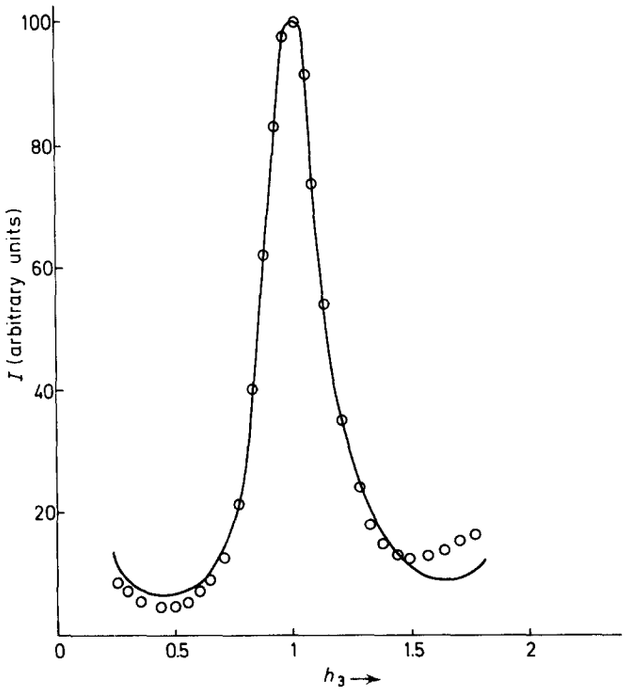

Figure 9 Observed (solid line) and calculated (circles) function $Z_3^2 S^2_3$

Table 2 Final macrolattice parameters

Macrolattice parameters	Unannealed polypropylene	Annealed polypropylene
B_3	–	900 Å
D_3	40 Å	135 Å
D_r	50 Å	85 Å
a_3	100 Å	255 Å
a_r	52 Å	75 Å
g_{33}	25%	9%
g_{r_3}	40%	14%
N_3	–	3.5
N_r	–	5
g_D	25%	19%
α_r	–	53%

direction increase remarkably whilst their thickness enlarges only from 50 to 85 Å. The equatorial interferences disappear because the lateral grain boundaries of the micro-para-crystals are no longer open after annealing. The lateral lattice constant of the macroparacrystal is therefore, according to *Table 2*, $a_r \sim 75$ Å. The volume crystallinity of each bundle is then given by

$$H_3/a_3 = 0.53 \pm 0.06 \qquad (45)$$

The value is within the experimental errors identical with the above mentioned value $\alpha_r = 0.577$ of the volume crystallinity and represents once again the proof for laterally closely packed microparacrystals.

Before annealing single microparacrystals lie in layer-like coherently scattering domains of $\sim 3 \times 3 \times 2 = 20$ pieces (*Figure 10a*). The lateral grain boundaries are so thick that reflections of their mean distances a_r appear on the equator[4] (see *Table 2*). These smectic-like domains grow remarkably during annealing up to $255 \times 3.5 = 900$ Å in the h_3-direction and $75 \times 5 = 375$ Å in

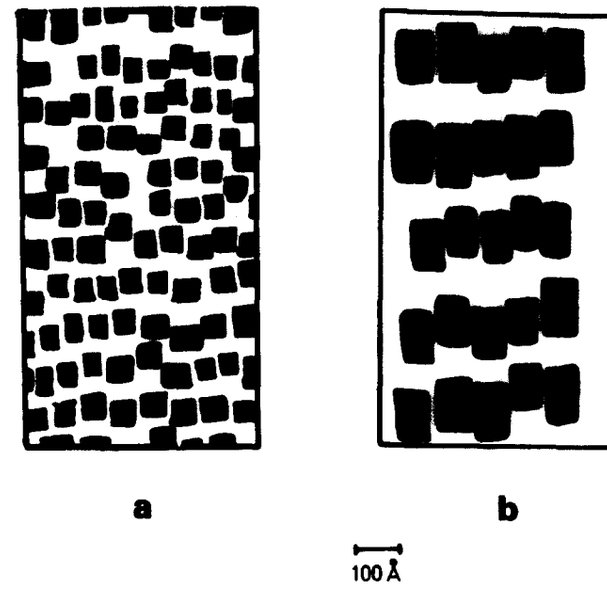

Figure 10 Bundles of microparacrystals in isotactic PP: (a) cold-drawn, (b) annealed

lateral direction. The microparacrystals grow laterally together in these domains (*Figure 10b*) and reach a very uniform length ($g_{33} = 0.09$). Nevertheless, they are shifted against each other ($g_{r3} = 0.14$). The structure is quite different from crystalline lamellae. In both cases the microparacrystals are the knots of a three-dimensional network of chain-segments connected in the fibre direction within the microparacrystals and between the single macroparacrystals. *Figure 10b* represents such a single macroparacrystal and *Figure 10a* about ten of them schematically.

ACKNOWLEDGEMENT

The authors are indebted to the Bundesanstalt für Materialprüfung (BAM), to the Freie Universität, Berlin, and to the Consiglio Nazionale delle Richerche, Bologna, who kindly supported this work.

APPENDIX

The integral width of a function consisting of Gaussian terms with maximum values α and $1-\alpha$ is given by

$$\delta^2 = \alpha\delta_1^2 + (1-\alpha)\delta_2^2$$

hence

$$\frac{1}{M_3^2} = \frac{\alpha}{(M'_3)^2} + \frac{1-\alpha}{(M''_3)^2}$$

$$= \frac{0.6}{4.8^2} + \frac{0.4}{11^1} = \frac{1}{5.6^2}$$

REFERENCES

1 Loboda-Čačković, J., Hosemann, R. and Čačković, H. *Kolloid-Z. Z. Polym.* 1971, **247**, 824
2 Wilke, W. and Weick, W. *Kolloid-Z. Polym.* 1972, **250**, 492
3 Ferracini, E., Ferrero, A., Loboda-Čačković, J., Hoseman, R. and Čačković, H. *J. Macromol. Sci.-Phys.* 1974, **B10**, 97
4 Loboda-Čačković, J., Hosemann, R., Čačković, H., Ferrero, A. and Ferracini, E. *Polymer* 1976, **17**, 303

5 Ferrero, A., Loboda-Čačković, J., Ferracini, E., Čačković, H. Proceedings V. International Conference on Small Angle Scattering, Berlin(1980)
6 Hermans, J. J. *Rec. Trav. Chim.* 1944, **63**, 5
7 Beumer, H. and Hoseman, R. *J. Macromol. Sci.-Phys.* 1978, **B15**(1), 1
8 Hosemann, R., Loboda-Čačković, J., Sassoui, M. and Weick, D. *Progr. Colloid. Polym. Sci.* 1979, **66**, 143
9 Yeh, G. S. Y., Hosemann, R., Loboda-Čačković, J. and Čačković, H. *Polymer* 1976, **17**, 309
10 Hosemann, R., Loboda-Čačković, J., Čačković, H., Fernandez-Bermudez, S. and Baltá-Calleja, F. J. *Z. Naturforsch.* 1979, **34c**, 112
11 Hosemann, R. *Phys. Scripta* 1982, **T1**, 142
12 Hosemann, R. *Polymer* 1962, **3**, 349
13 Hosemann, R., Hentschel, M. P., Baltá-Calleja, F. J., Lopez-Cabarcos, E. and Hindeleh, A. M. *J. Phys. Sol. Stat. Phys.* (in press)